Journal of Colloid and Interface Science 645 (2023) 775–783

Contents lists available at ScienceDirect

Journal of Colloid And Interface Science

journal homepage: www.elsevier.com/locate/jcis

Optimization of the wetting-drying characteristics of hydrophobic metal organic frameworks via crystallite size: The role of hydrogen bonding between intruded and bulk liquid

Liam J.W. Johnson [a,b,1], Gonçalo Paulo [c,1], Luis Bartolomé [a], Eder Amayuelas [a], Alberto Gubbiotti [c], Diego Mirani [d], Andrea Le Donne [e], Gabriel A. López [b], Giulia Grancini [d], Paweł Zajdel [f], Simone Meloni [e,*], Alberto Giacomello [c,*], Yaroslav Grosu [a,g,*]

[a] Centre for Cooperative Research on Alternative Energies (CIC energiGUNE), Basque Research and Technology Alliance (BRTA), Calle Albert Einstein, 48, Vitoria-Gasteiz, 01510, Araba/Alava, Spain
[b] Department of Physics, Faculty of Science and Technology, University of the Basque Country (UPV/EHU), Barrio Sarriena s/n, Bilbao, 48490, Leioa, Spain
[c] Dipartimento di Ingegneria Meccanica e Aerospaziale, Sapienza Università di Roma, Roma, Italy
[d] Department of Chemistry & INSTM University of Pavia, Via Taramelli 14, Pavia, I-27100, Italy
[e] Dipartimento di Scienze Chimiche e Farmaceutiche (DipSCF), Università degli Studi di Ferrara (Unife) Via Luigi Borsari 46, Ferrara, I-44121, Italy
[f] Institute of Physics, University of Silesia, 75 Pulku Piechoty 1, Chorzow, 41-500, Poland
[g] Institute of Chemistry, University of Silesia, Szkolna 9, Katowice, 40-006, Poland

ARTICLE INFO

Keywords:
Wetting-drying
Hydrogen-bonding
MOF
ZIF-8
HLS
Shock-absorbers

ABSTRACT

Hypothesis: The behavior of Heterogeneous Lyophobic Systems (HLSs) comprised of a lyophobic porous material and a corresponding non-wetting liquid is affected by a variety of different structural parameters of the porous material. Dependence on *exogenic* properties such as crystallite size is desirable for system tuning as they are much more facilely modified. We explore the dependence of intrusion pressure and intruded volume on crystallite size, testing the hypothesis that the connection between internal cavities and bulk water facilitates intrusion via hydrogen bonding, a phenomenon that is magnified in smaller crystallites with a larger surface/volume ratio.
Experiments: Water intrusion/extrusion pressures and intrusion volume were experimentally measured for ZIF-8 samples of various crystallite sizes and compared to previously reported values. Alongside the practical research, molecular dynamics simulations and stochastic modeling were performed to illustrate the effect of crystallite size on the properties of the HLSs and uncover the important role of hydrogen bonding within this phenomenon.
Findings: A reduction in crystallite size led to a significant decrease of intrusion and extrusion pressures below 100 nm. Simulations indicate that this behavior is due to a greater number of cages being in proximity to bulk water for smaller crystallites, allowing cross-cage hydrogen bonds to stabilize the intruded state and lower the threshold pressure of intrusion and extrusion. This is accompanied by a reduction in the overall intruded volume. Simulations demonstrate that this phenomenon is linked to ZIF-8 surface half-cages exposed to water being occupied by water due to non-trivial termination of the crystallites, even at atmospheric pressure.

1. Introduction

Natural and technological processes revolve around wetting – the interaction between fluids and solids. From self-cleaning leaves [1] and rapidly drying feathers [2] to the behavior of adhesives in bonded wood products [3] and new methods of gas storage [4], the wetting phenomenon plays a fundamental role in governing a wide range of mechanisms.

Controlled/selective wetting can be utilized for applications such as the separation of two liquids, the separation of a liquid-gas mixture, or indeed chromatography. Porous crystalline materials can preferentially retain one of the components of a mixture to facilitate separation. This

* Corresponding authors at: University degli Ferrara (Unife), Dipartimento di Ingegneria Meccanica e Aerospaziale, Sapienza Università di Roma, Centre for Cooperative Research on Alternative Energies (CIC energiGUNE), Basque Research and Technology Alliance (BRTA), Institute of Chemistry, University of Silesia.
E-mail addresses: simone.meloni@unife.it (S. Meloni), alberto.giacomello@uniroma1.it (A. Giacomello), ygrosu@cicenergigune.com (Y. Grosu).
[1] These authors contributed equally.

https://doi.org/10.1016/j.jcis.2023.04.059
Received 16 January 2023; Received in revised form 31 March 2023; Accepted 13 April 2023
Available online 23 April 2023

finds its roots in the intrusion/extrusion of materials into/from their pores.

Wettability is also fundamental to the penetration and evaporation of liquids in porous media. The process of a liquid entering into a previously vapor/gas-filled cage bounded by some walls is known as intrusion; the opposite process of water leaving the cages is extrusion. The pressures required to drive intrusion and extrusion are vital for the applicability of the system. For liquid separation [5–7], a lower intrusion pressure is preferred as cost can be reduced, whereas others, such as energy conversion, correlate a higher pressure with a greater quantity of energy stored per unit mass [8,9]. The intrusion/extrusion mechanism has many technological applications, amongst which are liquid phase chromatography [10,11], energy damping, conversion, and storage [12,13], porosimetry [14–16], biological and bioinspired channels [17–20], as well as the aforementioned and many more.

Both macroscopic [16,21–23] and microscopic [24,25] theories allow for the association of the intrusion and extrusion pressures with the presence of free energy barriers between the intruded and extruded states. For example, in spite of the fact that the free energy of the intruded state is lower than the extruded one, intrusion might be prevented by an energy barrier separating these two states (see Figure 1c-f of Lisi et al. [22]). In turn, the barriers depend on the characteristic size of the cages, on the surface chemistry, and on the topology [26] of the pores. More recently it has been shown that the intrusion/extrusion characteristics depend on the presence of small apertures in the pore walls, allowing the formation of hydrogen bonds across cages or with the bulk water outside the material [27,28].

To maximize the efficiencies of technologies based on hydrophobic MOFs and water, a greater understanding of the parameters that govern the intrusion/extrusion phenomenon is required. Of particular interest is the tuning of intrusion/ extrusion characteristics via the optimization of *exogenic* parameters, which do not require the modification of crystalline structure, pore size, grafting, etc. Following this approach, various contributors to this work have recently presented results that show that the tight packing of ZIF-8 crystallites into monolithic particles significantly alters the energy dissipated per water intrusion/extrusion cycle and, to some extent, the intrusion pressure itself [29].

Several works report the effect of crystallite size on the intrusion/extrusion pressures. Khay et al. explored the shape and size of MOF crystals and their effect on energetic performance, finding that an increase in crystallite size from nanoscale to microscale led to an increase in intrusion and extrusion pressure [30]. Two following works, Sun et al. [9] and Zajdel et al. [29], reported a similar trend: higher intrusion/extrusion pressures for larger crystallite size ZIF-8. Despite this being an intriguing opportunity to tune the intrusion/extrusion pressure by altering crystallite size [9,29,30], the mechanism behind this effect remains elusive.

In this work, by applying atomistic simulations, stochastic modeling, and water intrusion/extrusion experiments to several ZIF-8 samples of different sizes, we unexpectedly discovered the paramount role of hydrogen bonding between intruded and bulk water on the wetting characteristics of ZIF-8. Additionally, we have demonstrated the wetting behavior of the non-trivial termination of ZIF-8 crystals. These two insights allowed us to explain the effect of crystallite size on the wettability of ZIF-8 and propose it as an alternative approach for tuning the intrusion/extrusion pressure of hydrophobic MOFs without altering their chemistry and/or morphology.

2. Materials and methods

2.1. ZIF-8

The sample with the largest crystallite sizes, referred to as ZIF-8, was acquired from Merck as Basolite Z1200, CAS#59061-53-9.

2.2. nanoZIF-8a-c synthesis

The syntheses of the samples with nanoscale crystallite size, referred to as nanoZIF-8a, nanoZIF-8b and nanoZIF-8c, were performed according to a protocol already reported in the literature [31], which is further detailed in the Supporting Information.

2.3. Water porosimetry

ZIF-8 and nanoZIF-8 samples (a-c) were mixed with water and encapsulated into flexible, hermetic Teflon capsules prior to testing. High-pressure compression/decompression experiments were performed using an Auto Pore IV 9500 porosimeter (Micromeritics Instrument Corporation, Norcross, USA), where the penetrometer was evacuated to a pressure less than 7 Pa, followed by filling with mercury to 55 MPa. The system was compressed/decompressed in the required pressure range to observe the intrusion/extrusion phenomenon. Each material was evaluated with a minimum of three compression/decompression cycles.

2.4. X-ray diffraction

A Bruker D8 Discover X-ray diffractometer was used with a LYNXEYE-XE detector using CuKα1 radiation ($\lambda = 1.5418$ Å) and Bragg-Brentano θ:2θ geometry. The data collection was conducted at room temperature, between 5° and 40° with a step of 0.02° and a dwell time of 2 s per step. Crystallite size (coherent domain size) was estimated using the LeBail [32] method implemented in Fullprof Suite [33]. ZIF-8 patterns were generated assuming ideal cubic symmetry with space group I -43m (#217) and laue class m-3m. The diffraction peaks were visibly broadened in comparison to the standard pattern of Al_2O_3, which was used to measure the machine resolution function. The quantitative analysis of the size broadening was achieved using the spherical harmonics formalism defined by Järvinen [34]. The model for Laue class m-3m possesses only 5 parameters: K00, K41, K61, K62, K81, from which only the first 2 were used. Possible strain effects were modeled using the parametric approach introduced by Stephens et al [35]. The refined patterns and the data are presented in Figure S1 and Table S2, respectively.

2.5. Molecular dynamics simulation

Classical Molecular Dynamics simulations were conducted using the LAMMPS code [36] using the force field for the ZIF-8 proposed by Zheng et al. [37] in combination with the TIP4P/2005 model of water [38]. The interactions between ZIF-8 and water were calculated via electrostatic potentials plus the modified $4\epsilon[(\sigma/r)^{12} - c(\sigma/r)^6]$ Lennard-Jones interaction to tune the hydrophobicity of ZIF-8 [39]. This setup has already been successfully used in the previous work of some of the co-authors of this manuscript [29,40]. Three different computational samples of ZIF-8 were investigated: the first system is a tri-periodic 2 x 2 x 2 supercell containing 640 water molecules, 40 water molecule per cage. With this computational sample we compute the effect of hydrogen bond bridging across 6 MR apertures, as measured by the average value and distribution of the potential energy and the “effective” contact angle of inner ZIF-8 surface. Here, the contact angle does not have to be understood in the geometrical sense, as the angle formed by a droplet deposited on ZIF-8 cages. Rather, in the present case the contact angle is just a convenient measure of the dependence of the repellence of ZIF-8 inner surface for water, its hydrophobicity, on the possibility to form hydrogen bonds across 6 MR apertures. For computing this “effective” contact angle we rely on the Young–Duprè equation, already used in the past in atomistic simulations [41]. This required the calculation of the energy of separated bulk ZIF-8 and water, plus the wet ZIF-8 sample mentioned here. Concerning the size of the system, for an accurate estimate of these energies it is sufficient that the simulation box is large enough to allow a proper calculation of the real space

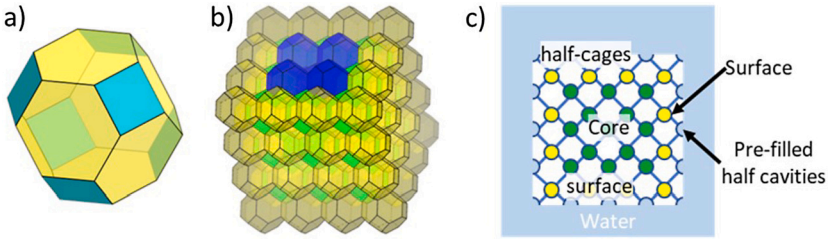

Fig. 1. a) Truncated octahedral ZIF-8 cages: 6-membered ring (6 MR) and 4-membered ring (4 MR) windows are represented in yellow and cyan respectively. 6 MR are large enough to let water molecules pass through, whereas 4 MR are considered too narrow. b) the cubic ZIF-8 crystallite. Surface and core cages are indicated in yellow (transparent) and green respectively. Four surface cages and one subsurface cage combine to form top half-cages. c) 2D cartoon of the cubic crystallite systems used to develop the stochastic model of intrusion/extrusion. The crystallites are made of cages, here represented by circles, connected along the (111) direction. One identifies three types of cages: i) surface half-cages, colored in light blue, the same color used for water in order to highlight that they are pre-filled; ii) surface cages (yellow), where hydrogen bonds form across 6 MR apertures with water in the pre-filled half cages; iii) core cages (green), which might or might not form hydrogen bonds across 6 MR apertures depending on whether the neighboring cages are intruded. (For interpretation of the colors in the figure(s), the reader is referred to the web version of this article.)

part of the Ewald sum to solve electrostatic interactions, and our sample, ~ 3.5 x 3.5 x 3.5 nm, is significantly larger than twice this cutoff, 1.3 nm.

The second one is a 7-unit cell-thick slab (~ 19.0 nm), with a 2 x 2 di-periodic surface extending in the x-y plane (~ 3.5 x 3.5 nm) and 5200 water molecules. Furthermore, this system has already been used in previous works [40] and the sample is large enough for the correct computation of electrostatics. Moreover, the state of the system for which we computed the single cage intrusion free energy barrier has been selected from previous extensive simulations of the overall intrusion in a slab [40], hence the sample is a realistic representation of the system along the process. The single cage intrusion free energy barrier is computed using the restrained molecular dynamics technique, discussed in detail in the Supplementary Material. In practice, here we run 41 independent simulations of a duration of ~ 4 ns with an increasing number of water molecules in the selected ZIF-8 cage. From these simulations we estimate the derivative of the free energy along the process, which is then numerically integrated using the trapezoid rule.

The third sample consists of a 2 x 8-unit cells wide slab, with a thickness of 4 unit cells. This sample has been used to investigate the wetting of surface half-cages before the application of any pressure. As in the other cases, the sample is large enough to allow a proper calculation of interatomic forces, including the real-space contribution to long range electrostatics. On this slab we deposit either a liquid droplet (3000 molecules) or a film (~ 5300 molecules).

2.6. Stochastic models

The ZIF-8 crystal was presented in a lattice model, as described in Fig. 1. To mimic the inter-cage interactions of ZIF-8, we chose to have each lattice site interact with its diagonal neighbors instead of with those that were directly adjacent.

Each site of the square lattice had two different states, filled or empty, corresponding to the filled or empty ZIF-8 crystal cage states. Following the capillary theory of wetting/drying of hydrophobic pores [23] and the observations reported in the main text on the effective hydrophobicity of hydrogen bonding across 6 MR apertures, the rate of filling of an initially empty site, or the reverse, depends on the state of the neighboring sites and the applied pressure. Here, we consider that the average time of filling/emptying a ZIF-8 cage, $t_{f/e}$, can be expressed with an Arrhenius-like law:

$$t_f = t_f^0 e^{\frac{\Omega_f}{k_B T}} \quad (1)$$

$$t_e = t_e^0 e^{\frac{\Omega_e}{k_B T}} \quad (2)$$

Where $t_{f/e}^0$ is the characteristic time of filling/emptying, $\Omega_{f/e}$ is the filling/emptying barrier, and $K_B T$ is the thermal energy at operative conditions, with K_B is the Boltzmann constant and T is temperature. For the sake of simplicity, we considered t_f^0 and t_e^0 to be the same and independent of pressure. This may not always be true, but an empirical analysis of their effect on the *in silico* liquid porosimetry revealed that the key qualitative findings are independent of their values (see supporting information).

The probability that a transition from a filled state to a dry state or from a dry state to a filled state is given by the equations:

$$p_f = 1 - e^{-dt/t_f} \quad (3)$$

$$p_e = 1 - e^{-dt/t_e} \quad (4)$$

where dt is the time interval used for integration. Further details on the specific values used in this work are reported in the supporting information.

3. Results and discussion

3.1. Experimental observations of the crystallite size effect on water intrusion/extrusion pressure and intrusion volume of ZIF-8

ZIF-8 is an iconic example of a hydrophobic MOF with Sodalite type topology (SOD) (Fig. 1): stable, well-researched, and the first commercial hydrophobic MOF. Several samples of nanoZIF-8 of various crystallite sizes (henceforth denoted as a, b, and c – see SI for synthesis protocols and Figures S1-S6 for their characterization) were synthesized before being subjected to water intrusion/extrusion experiments. These data were complemented with other crystallite sizes that have been reported in the literature [9,29,30] to give a comprehensive exploration of the relationship between crystallite size and intrusion/extrusion characteristics.

Fig. 2 shows the effect of crystallite size on the intruded volume, and intrusion and extrusion pressures. Liquid porosimetry and literature data (Fig. 2a-b) report a reduction in intrusion and extrusion pressures when the crystallite size falls below 500 nm: it is easier to intrude into the material, but harder to extrude from it, although the extrusion pressure remains well above atmospheric pressure. Despite the order of magnitude difference in crystallite size and the shifts in intrusion and extrusion pressures, the hysteresis of the system appears constant at ~4 MPa within the explored range of crystallite sizes. Some scattering observed in Fig. 2a-b can be due to differences in ZIF-8 samples (synthesis protocols), water purity, equipment, testing conditions (compression/decompression rate, for example) used by different research groups.

First, we examine if the observed trend (Fig. 2a-b) could be due to the effect of crystallite size on the flexibility of ZIF-8. Tian et al. [42] and Tanaka et al. [43] have discussed the alteration of ZIF-8 flexibility with a change of grain size and therefore the effect on the free movement of mIM (the gate-opening). This reduction in mobility is associated

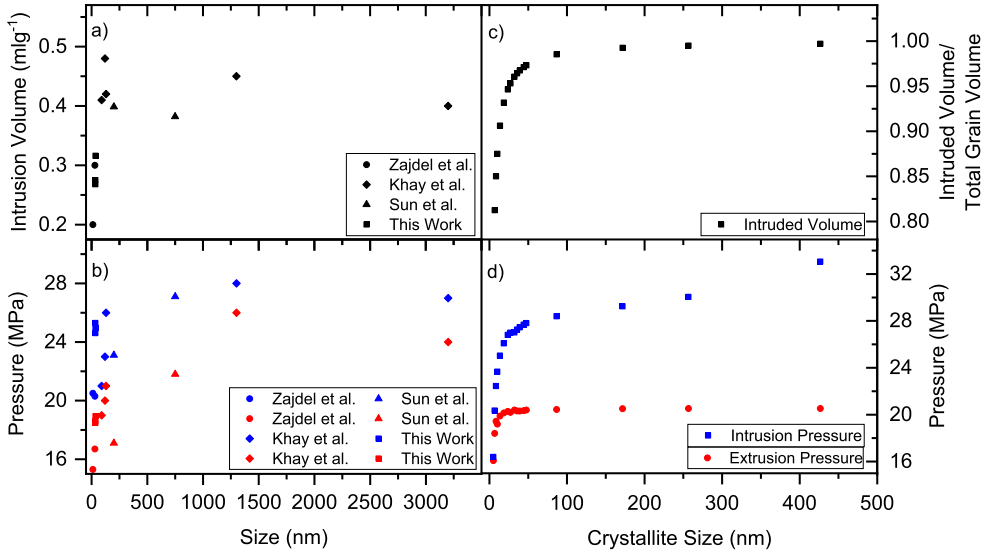

Fig. 2. The dependence of water intrusion/extrusion pressure and intruded volume with crystallite size of ZIF-8. Experimental data show that there is a steep dependence of both the intruded volume (a) and the intrusion (blue) and extrusion (red) pressures (b) on the crystallite size below 500 nm. These results are compiled from four different works [9,29,30] including this one. Panels (c) and (d) show the steep dependence of intruded volume (c) and intrusion/extrusion pressures (d) from stochastic modeling on the size of the grid. When considering the intruded volume, the surface of the crystal is not included because, as demonstrated experimentally, the surface termination of ZIF-8 does not constitute a pore. This gives rise to the dependence seen in panel (c), with the intruded volume eventually stabilizing as the surface contributions become negligible in comparison to the overall volume. Panel (d) also shows the importance of the surface contributions to the reduction of the intrusion/extrusion pressure at smaller crystallite sizes, and indeed the increase at larger crystallite sizes, as the surface contribution becomes smaller.

with a higher energy penalty to permit the structural transition for the additional uptake of Ar and N_2 molecules. Similarly, higher pressure is required to intrude water into stiffened ZIF-8 (J. D. Littlefair, 2023, in preparation). Considering that smaller crystallite size results in stiffer ZIF-8 [29], the trend of P_{int} with size in Fig. 2b is the opposite of what is expected from the flexibility effect: crystallite-size-induced stiffening should result in a higher intrusion pressure. Thus, the effect of flexibility appears to be overshadowed by another effect, which is solely and directly related to size. For this reason, it was neglected in the subsequent analysis.

The system is incredibly complex, with some of the properties having been investigated in a previous paper by some of the co-authors of this work [29]. Gas adsorption and mercury porosimetry techniques were used for porosity characterization in these samples. Moreover, as has been previously mentioned, the extreme case of agglomeration (a monolith) was studied in this reference, and some effects due to the textural characteristics were witnessed. These effects were *not* taken into account by the stochastic model, and yet in spite of this, this system captures the effect of crystallite size on the intrusion/extrusion characteristics that was found experimentally. Thus, we hypothesize that the observed trends in intrusion/extrusion pressures and intrusion volume are predominantly a consequence of crystallite size. Indeed, the very fact that the model is relatively simplistic, whilst capturing the main effects of the system, makes it even more useful as the computational cost is reasonable.

The distribution of water within the ZIF-8 cages has been previously investigated by Wolanin et al. [44] and by some of the co-authors of this work in Tortora et al. [40]. Figure SI7 from the supporting information of Tortora et al. [40] indicates the presence of water molecules in close proximity to the 6 MR windows, which should be energetically unfavorable, but is indeed stabilised by the hydrogen-bonding that can take place across the window.

In spite of the fact that ZIF-8 is hydrophobic, once intruded, there is a degree of textural changes caused by swelling, and indeed there is an effect of crystallite size on the degree of this inflation. Some of the co-authors of this work have already conducted some *in operando* structural analysis experiments on ZIF-8 [40] and on other MOFs [45] upon water intrusion/extrusion.

In figure 1a-b of Tortora et al. [40] one can clearly see a pronounced swelling of the framework as water intrusion takes place. This expansion of the lattice during liquid intrusion is the result of two phenomena: rotation of ZnIm4 tetrahedra (where Im stands for 2-methylimidazole) and stretching of the bonds (see Figure 1h and Figure SI6 in Tortora et al.). These processes are mainly induced by water molecules occupying the pseudohexagonal windows joining ZIF-8 cavities (see Figure SI7 in Tortora et al.), thus pushing apart the corresponding Im ligands and Zn atoms associated with them.

As has been alluded to already, there are many factors that could contribute to this effect. In order to have as much information as possible, a comprehensive approach was adopted, with laboratory experiments, molecular dynamics simulations, and most importantly the stochastic model which, despite its simplicity, is able to capture the experimentally observed effect of crystallite size. The fact that this model captures this effect on the intrusion/extrusion pressures and intrusion volume suggests that the observed trends are primarily related to crystallite size.

3.2. *Molecular dynamics simulations of the ZIF-8 + water system*

From high resolution TEM characterization of ZIF-8, it is known that the termination of its crystal is not trivial and half-cages are observed on the crystal surface [46]. To capture this observation, a MD simulation campaign was performed using ZIF-8 surfaces terminated with such half-cages. A key result presented here is that, despite the hydrophobicity of the material, the half-cages present on the surface, which are exposed to bulk water, are filled with liquid, as illustrated in Fig. 3. Figure S10 in the Supporting Information shows that this is not due to the liquid being deposited as a droplet; the same phenomenon is observed when one places a liquid film on the same, overall hydrophobic ZIF-8 surface. In other words, these half-cages are already wet at ambient conditions and therefore do not contribute to the intruded volume at the intrusion pressure.

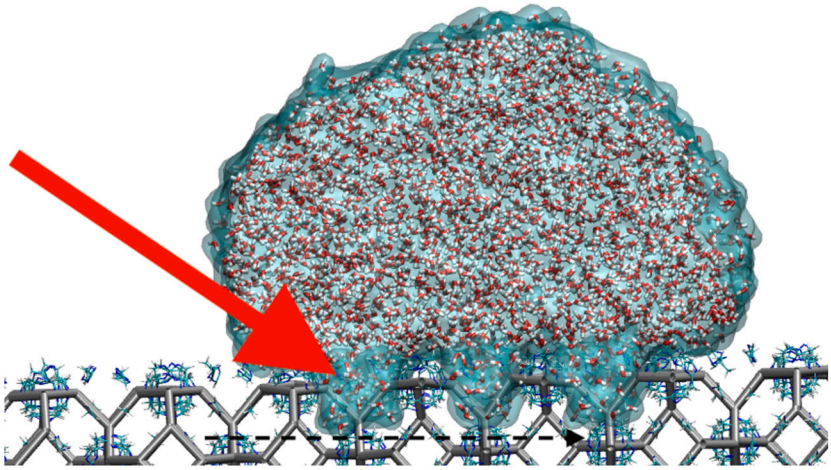

Fig. 3. Water contact angle on the ZIF-8 surface. Despite the hydrophobicity of ZIF-8, confirmed by a contact angle > 90°, surface half-cages are filled with water. This allows for hydrogen bonds between water in the surface cages and the bulk liquid.

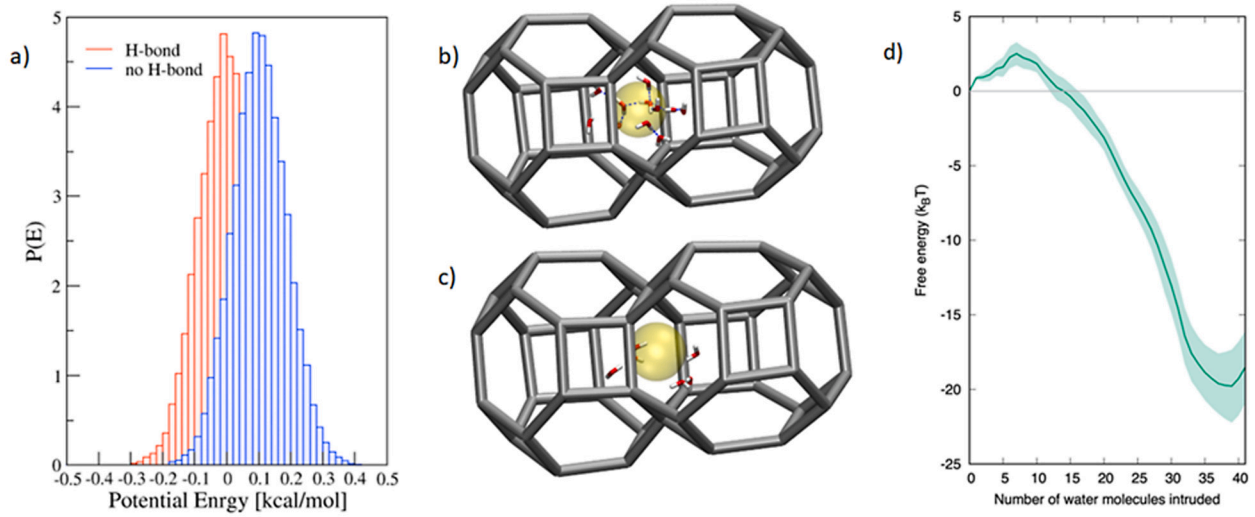

Fig. 4. Distribution of the potential energy per water molecule in the samples where hydrogen bonding across 6 MR apertures is allowed (red – see also panel b) and forbidden (blue – see also panel c). Energies are shifted so that the average value of the potential energy per atom of the sample where hydrogen bonding across 6 MR is allowed is equal to zero. This allows us to focus on the difference of potential energy between the two samples. One notices that the two distributions are shifted by ~ 0.2 kcal/mol, confirming that the stabilization effect of hydrogen bond across 6 MR apertures is non-negligible. Panels b and c show a snapshot taken along MD for the cases in which hydrogen bonds across 6 MR are allowed and forbidden respectively. When not forbidden, hydrogen bonding occurs, with water molecules approaching the center of the 6 MR aperture despite its narrow size, highlighted in yellow. d) The free energy profile of the water intrusion in a single ZIF-8 cavity in the core region of the computational slab. The shadow around the line represents the statistical error associated with the free energy calculation, determined by the limited duration of the simulation (see SI for a detailed discussion). It is of note that an energy barrier of ~ 2.5 k_BT must be overcome for intrusion.

The fact that the surface cages are filled with water allows us to explain the intrusion volume trend (Fig. 2a and 2c) by deriving a mathematical relation between the crystallite size and the intrusion volume per unit mass of the MOF, which, for cubic crystallites (Fig. 1), is found in equation (5), where V is the intruded volume of a crystallite comprising N cages, V_∞ is the corresponding volume per unit mass of the MOF of an infinite crystallite, and m is the mass of the crystallite. A complete derivation of this formula is presented in Section 3 of the Supporting Information: the key element is to consider that only the volume of the internal cages contributes to the intrusion volume, while atoms forming pre-filled top cages contribute to the mass of the crystallite.

$$\frac{V}{m} = \frac{1 - \frac{3}{2N} V_\infty}{m} \tag{5}$$

To explain the origin of the reduction of the intrusion pressure with crystallite size, it is convenient to summarize the results recently reported in the literature. Water molecules within the cage form hydrogen bonds across the 6-membered ring (6 MR) apertures with water molecules outside, either in neighboring cages or in the outer, pre-filled half-cages [40]. These cross-cage hydrogen bonds stabilize the intruded state. This is shown by the comparison between the potential energy of water embedded in a ZIF-8 sample when cross-cage hydrogen bonding is allowed or forbidden (Fig. 4a-c, see supporting information for computational details). To express this differently, following Bushuev et al., cross-cage hydrogen bonding lowers the effective hydrophobicity of ZIF-8, which, in turn, reduces both the intrusion and extrusion pressures [27,47]. Following the approach introduced by Caddeo et al. [41], based on the Young-Duprè equation, we show that the effective contact angle of ZIF-8 goes from 114° when cross-cage hydrogen bonding is forbidden to 101° when it is allowed (see Supporting Information Section 4 Table S2).

Thus, surface ZIF-8 cages (the first layer of the complete cages immediately in contact with external water through the pre-filled surface half-cages (Fig. 1c, yellow cages)) are easier to intrude as their effective

hydrophobicity is lower. This suggests that in smaller crystallites, characterized by a larger surface/volume ratio, intrusion is easier, and the corresponding pressure is reduced.

Our simulations reveal that at 50 MPa (the theoretical intrusion pressure for the atomistic model used in the simulations [40]), the intrusion barrier of a single cage is ~5 k_BT, i.e., five times the thermal energy at room temperature, Fig. 4d. Following Giacomello et al. [48], the intrusion barrier reduces with increasing pressures, while the opposite extrusion barrier decreases at lower pressures [27]. Due to hydrogen bonding across the 6 MR apertures, the intrusion barrier of a cage, and thus its intrusion probability, depends on the number of already intruded nearest neighboring cages: the greater the number of neighboring cages that are already intruded, the lower the intrusion barrier and thus the higher the intrusion probability at a given time.

3.3. Stochastic modeling of the crystallite size effect on water intrusion/extrusion pressure and intrusion volume of ZIF-8

The experimental results (Fig. 2a-b) were interpreted in terms of a stochastic model, which captured clearly the main experimental trends (Fig. 2c-d) as well as details of the intrusion/extrusion cycle (Fig. 5a vs 3b). For a detailed description of the model, see section 2 of the Supporting Information. Briefly, we presented the ZIF-8 crystal in a lattice model, as described in Fig. 1. The main assumptions, which were introduced into this model are as follows:

1. The filling and emptying of the cages of the ZIF-8 crystal can be modeled using a stochastic process.
2. Surface cages of the ZIF-8 crystal (Fig. 1b) are filled with water under ambient pressure. Therefore, they do not contribute to the intrusion/extrusion volume at high pressure.
3. The probability of each cage to get intruded by water at high pressure is proportional to the number of neighboring cages that are already wet.

The first assumption is discussed in the Stochastic Model methods subsection, whilst the other two arise from the independent atomistic simulations described above in the MD Simulations subsection.

In Fig. 5, we compare experimental a) and *in silico* b) liquid porosimetry results; the latter of which was obtained by the stochastic model. As in the experiments, this simple model reproduces the increase of the intrusion and extrusion pressures with the size of the crystallite. Since they are based on the same hypotheses, the model also produces a trend of the intruded volume with crystallite size consistent with the theoretical equation derived above, and both are consistent with the experimental trend. Remarkably, the stochastic model applied to samples of same volume but different shape (cubic, prolate, oblate) returns almost indistinguishable liquid porosimetry results (see Figure S8), confirming that it is the volume of the crystallite the key property governing the intrusion/extrusion characteristics of the material. This analysis also shows the key role of pre-wet surface half cages in driving intrusion (see Supplementary Information).

One notices that the stochastic model does not completely capture the slopes associated with the intrusion and extrusion process nor the almost constant hysteresis observed experimentally, as the model shows a larger change in the intrusion pressure than it does in the extrusion pressure. These differences can be attributed to the simplifications used for computing the probabilities that govern the stochastic model, the much greater pressure scanning rates that are necessary in simulations due to the high computational costs, the shape and characteristics of crystallites in the experimental sample, as well as the size distribution. Conversely, in this model an ideal monodispersed sample was considered. However, these details are a matter of fine-tuning the stochastic model to better match the experimental results.

The consistency between the experimental results and our simple model confirms the hypothesis discussed above: the relationship between the intrusion and extrusion pressures and the crystallite size is due to the (relatively) greater number of surface cages in smaller crystallites, which are more easily intruded because of the hydrogen bonding across the 6 MR apertures with bulk water. This interpretation is confirmed by the observation that the outer cages are filled first (Supporting Information, Figure S8) before the liquid proceeds towards the center of the crystallite, which occurs as they are in contact with already filled surface half-cages prior to the application of hydrostatic pressure.

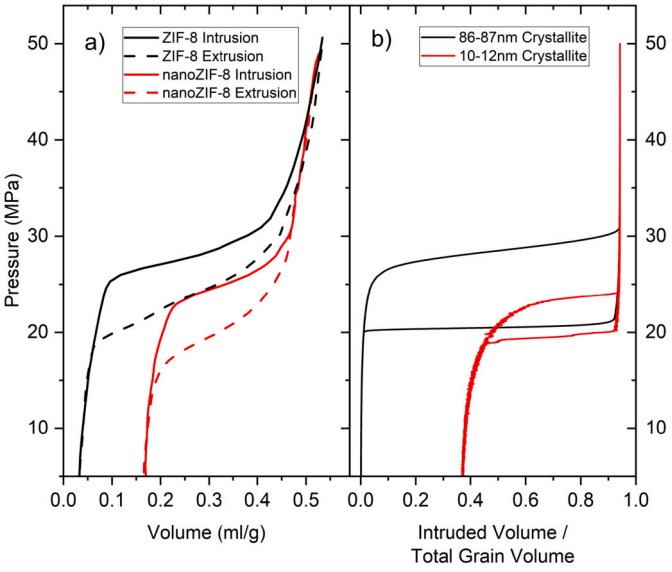

Fig. 5. a) experimental and b) calculated water intrusion/extrusion cycles for ZIF-8 of different crystallite dimensions. For a), the solid line represents intrusion, and the dashed line represents extrusion. Different crystallite sizes of ZIF-8 yield different intrusion/extrusion pressures and total intruded volume. For regular ZIF-8, in black, where the crystallite size is ~300 nm, the intrusion pressure is 27 MPa and the extrusion pressure is 23 MPa. nanoZIF-8, in red, which has a crystallite size of ~35 nm, has a lower intrusion pressure of 22 MPa and a lower extrusion pressure of 18 MPa. b) PV isotherms of two systems: one is made of 10 x 10 x 10 cages and thus has dimensions that are 10 times the unit cell of ZIF-8 (~ 17 nm), whereas the other is a model for a crystallite of 170 nm in length. In both cases, the curves are displaced along the x-axes for ease of comparison, and the intrusion pressure is extracted at $V_{int}/2$.

Conversely, extrusion requires a lower pressure (extrusion is less favorable) and the process starts from the center of the crystallite: extrusion of the outer cages is more difficult, and requires a lower pressure, for the same reason: they are in contact with pre-filled surface half-cages, allowing hydrogen bonds between intruded and bulk water to stabilize the intruded state. Incidentally, the consistency of the experimental and theoretical trend is the first experimental validation of the theory recently proposed [27,47] that hydrogen bonding across narrow apertures connecting the cages of porous materials with others and with bulk water facilitates intrusion.

4. Conclusion

Based on new experiments and recently reported data on ZIF-8 [9, 29,30] this work has demonstrated that the wetting-drying of ZIF-8 can be tuned using the *exogenic* property of crystallite size, thus making it a viable option for a greater number of applications, such as shock-absorber technology. As ZIF-8 synthesis is a simple process and it is already a commercial product, this makes it a perfect candidate for technological applications, as it does not require the development of novel lyophobic nanoporous and sub-nanoporous materials, and can be readily tuned *via* simple modifications to the synthesis protocol [58,59].

Comparison to literature data in Table 1[9,29,30,49–57] illustrates the advantages of the nanoZIF-8 systems, demonstrating much lower

Table 1
A summary of the results from this study [*] and previous investigations conducted by Sun et al. [9], Zajdel et al. [29], Khay et al. [30,57], Grosu et al. [49], Ronchi et al. [50,52–56], and Ryzhikov et al. [51] Crystallite sizes for samples nanoZIF8a-c were established from the Lebail refinement of XRD analyses (See Table S1 and Figure S1) and TEM images (Figure S2-S5). Intrusion pressure, extrusion pressure, and intrusion volume for HLSs comprised of samples nanoZIF-8a-c were calculated from the intrusion curves (Figure S6).

	Size (nm)	P_{int} (MPa)	P_{ext} (MPa)	V_{int} (ml/g)	Ref.
mono_nanoZIF-8	12	20.5	15.3	0.20	[29]
powder_nanoZIF-8	30	20.3	16.7	0.30	[29]
NRD-ZIF-8	90	21.0	19.0	0.41	[30]
NS-ZIF-8	120	23.0	20.0	0.48	[30]
NC-ZIF-8	130	26.0	21.0	0.42	[30]
MRD-ZIF-8	3200	27.0	24.0	0.40	[30]
MCTE-ZIF-8	1300	28.0	26.0	0.45	[30]
bigger ZIF-8	750	27.1	21.8	0.38	[9]
smaller ZIF-8	200	23.1	17.1	0.40	[9]
ZIF-8	300	28.0	22.5	0.41	[*]
nanoZIF-8a	34	24.6	18.5	0.28	[*]
nanoZIF-8b	34	25.3	18.6	0.27	[*]
nanoZIF-8c	35	25.0	18.9	0.32	[*]
Cu_2(tebpz) MOF	-	35.7	35.4	0.12	[49]
DDR	-	60.0	51.0	0.11	[50]
LTA	-	20.0	-	0.17	[51]
CFI	-	75.0	75.0	0.08	[52]
DON	-	26.0	21.0	0.04	[52]
MTF	-	125.0	125.0	0.01	[53]
FER	-	150.0	143.0	0.06	[54]
CDO	-	210.0	180.0	0.03	[53]
ITH	-	82.0	-	0.08	[55]
BEC	-	41.0	-	0.08	[56]
MFI	-	96.0	95.0	0.10	[57]

intrusion/extrusion pressures compared to other materials, with the exception of DON [52] and LTA [51]: the former having a very low intrusion volume and the latter not extruding water after intrusion, rendering it incapable of cycling.

Our theoretical analysis identified the microscopic origin of the intrusion pressure dependence on crystallite size, which is made easier by the already wetted surface half-cages: water in these half-cages facilitates intrusion by the formation of hydrogen bonds with intruding water molecules, stabilizing the intruded states. Since in smaller crystallites the surface/volume ratio is larger, this effect is magnified and intrusion pressure is significantly reduced. For the same reasons, extrusion pressure is also reduced in small crystallites.

Moreover, in this work we develop a comprehensive theory of the intrusion/extrusion of liquids in lyophobic materials and provide a stochastic model to simulate PV-intrusion/extrusion cycles of crystallites of size comparable to those studied experimentally. Despite the simplicity of the stochastic model, it accurately captures the effect of crystallite size on the intrusion/extrusion characteristics. In the future, we plan to generalize this theory and model to other porous materials with different geometries, to provide the computational tools required for the advanced design of heterogeneous lyophobic systems based on nanoporous materials and non-wetting liquids.

CRediT authorship contribution statement

Liam J.W. Johnson: Formal analysis, Investigation, Visualization, Writing – original draft. **Gonçalo Paulo:** Formal analysis, Investigation, Methodology, Visualization, Writing – review & editing. **Luis Bartolomé:** Formal analysis, Investigation. **Eder Amayuelas:** Formal analysis, Investigation. **Alberto Gubbiotti:** Formal analysis, Investigation, Methodology. **Diego Mirani:** Formal analysis, Investigation. **Andrea Le Donne:** Formal analysis, Investigation, Visualization. **Gabriel A. López:** Writing – review & editing. **Giulia Grancini:** Methodology, Supervision. **Paweł Zajdel:** Formal analysis, Investigation, Methodology, Visualization, Writing – review & editing. **Simone Meloni:** Conceptualization, Methodology, Project administration, Supervision, Writing – review & editing. **Alberto Giacomello:** Conceptualization, Methodology, Project administration, Supervision, Writing – review & editing. **Yaroslav Grosu:** Conceptualization, Methodology, Project administration, Supervision, Writing – review & editing.

Declaration of competing interest

The authors declare that they have no known competing financial interests or personal relationships that could have appeared to influence the work reported in this paper.

Data availability

Data will be made available on request.

Acknowledgements

This project has received funding from the European Union's Horizon 2020 research and innovation program under grant agreement No.101017858. This research is part of a project that has received funding from the Eropean Research Council (ERC) under the European Union's Horizon 2020 research and innovation program (grant agreement No. 803213). The authors acknowledge PRACE for awarding us access to Marconi100 at CINECA, Italy. LJ would like to acknowledge Yagmur Polat for her assistance preparing XRD samples.

Appendix A. Abbreviations

MOF	Metal-organic Framework
HLS	Heterogeneous Lyophobic System
ZIF	Zinc Imidazole Framework
SOD	Sodalite type zeolites
6 MR	6-membered ring
4 MR	4-membered ring
P_{int}	Intrusion Pressure
P_{ext}	Extrusion Pressure
V_{int}	Intrusion Volume

Appendix B. Supplementary material

Supplementary material related to this article can be found online at https://doi.org/10.1016/j.jcis.2023.04.059.

References

[1] M. Zhang, S. Feng, L. Wang, Y. Zheng, Lotus effect in wetting and self-cleaning, Biotribology 5 (2016) 31–43, https://doi.org/10.1016/j.biotri.2015.08.002, publisher: Elsevier Ltd.
[2] Y. Liu, X. Chen, J.H. Xin, Hydrophobic duck feathers and their simulation on textile substrates for water repellent treatment, Bioinspir. Biomim. 3 (2008) 8, https://doi.org/10.1088/1748-3182/3/4/046007.
[3] J. Rathke, G. Sinn, Evaluating the wettability of MUF resins and pMDI on two different OSB raw materials, Eur. J. Wood Prod. 71 (3) (2013) 335–342, https://doi.org/10.1007/s00107-013-0675-6.
[4] M. Ali, N. Yekeen, N. Pal, A. Keshavarz, S. Iglauer, H. Hoteit, Influence of pressure, temperature and organic surface concentration on hydrogen wettability of caprock, implications for hydrogen geo-storage, Energy Rep. 7 (2021) 5988–5996, https://doi.org/10.1016/J.EGYR.2021.09.016, publisher: Elsevier.
[5] P. Bai, M.Y. Jeon, L. Ren, C. Knight, M.W. Deem, M. Tsapatsis, J.I. Siepmann, Discovery of optimal zeolites for challenging separations and chemical transformations using predictive materials modeling, Nat. Commun. 6 (1) (2015) 1–9, https://doi.org/10.1038/ncomms6912, publisher: Nature Publishing Group.
[6] A.K. Kota, G. Kwon, W. Choi, J.M. Mabry, A. Tuteja, Hygro-responsive membranes for effective oil–water separation, Nat. Commun. 3 (1) (2012) 1–8, https://doi.org/10.1038/ncomms2027, publisher: Nature Publishing Group.
[7] H.C. Yang, J. Hou, V. Chen, Z.K. Xu, Janus membranes: exploring duality for advanced separation, Angew. Chem., Int. Ed. Engl. 55 (43) (2016) 13398–13407, https://doi.org/10.1002/ANIE.201601589, publisher: John Wiley & Sons, Ltd.

[8] I. Khay, G. Chaplais, H. Nouali, G. Ortiz, C. Marichal, J. Patarin, Assessment of the energetic performances of various ZIFs with SOD or RHO topology using high pressure water intrusion–extrusion experiments, Dalton Trans. 45 (2016) 4392–4400, https://doi.org/10.1039/C5DT03486H, publisher: The Royal Society of Chemistry.
[9] Y. Sun, S.M. Rogge, A. Lamaire, S. Vandenbrande, J. Wieme, C.R. Siviour, V. Van Speybroeck, J.C. Tan, High-rate nanofluidic energy absorption in porous zeolitic frameworks, Nat. Mater. 20 (7) (2021) 1015–1023, https://doi.org/10.1038/s41563-021-00977-6, publisher: Nature Research.
[10] S.R. Bakalyar, M.P. Bradley, R. Honganen, The role of dissolved gases in high - performance liquid chromatography, J. Chromatogr. A 158 (C) (1978) 277–293, https://doi.org/10.1016/S0021-9673(00)89973-2, publisher: Elsevier.
[11] F. Gritti, D. Brousmiche, M. Gilar, T.H. Walter, K. Wyndham, Kinetic mechanism of water dewetting from hydrophobic stationary phases utilized in liquid chromatography, J. Chromatogr. A 1596 (2019) 41–53, https://doi.org/10.1016/j.chroma.2019.02.051.
[12] Y. Grosu, M. Mierzwa, V.A. Eroshenko, S. Pawlus, M. Chorazewski, J.M. Nedelec, J.P.E. Grolier, Mechanical, thermal, and electrical energy storage in a single working body: electrification and thermal effects upon pressure-induced water intrusion-extrusion in nanoporous solids, ACS Appl. Mater. Interfaces 9 (8) (2017) 7044–7049, https://doi.org/10.1021/acsami.6b14422, publisher: American Chemical Society.
[13] V. Eroshenko, R.C. Regis, M. Soulard, J. Patarin, Energetics: a new field of applications for hydrophobic zeolites, J. Am. Chem. Soc. 123 (33) (2001) 8129–8130, https://doi.org/10.1021/JA011011A, publisher: American Chemical Society.
[14] R. Helmy, Y. Kazakevich, C. Ni, A.Y. Fadeev, Wetting in hydrophobic nanochannels: a challenge of classical capillarity, J. Am. Chem. Soc. 127 (36) (2005) 12446–12447, https://doi.org/10.1021/JA053267C, publisher: American Chemical Society.
[15] B. Coasne, A. Galarneau, F.D. Renzo, R.J. Pellenq, Intrusion and retraction of fluids in nanopores: effect of morphological heterogeneity, J. Phys. Chem. C 113 (5) (2009) 1953–1962, https://doi.org/10.1021/JP807828A, publisher: American Chemical Society.
[16] A. Tinti, A. Giacomello, Y. Grosu, C.M. Casciola, Intrusion and extrusion of water in hydrophobic nanopores, Proc. Natl. Acad. Sci. USA 114 (48) (2017) E10266–E10273, https://doi.org/10.1073/pnas.1714796114, publisher: National Academy of Sciences.
[17] R. Roth, D. Gillespie, W. Nonner, R.E. Eisenberg, Bubbles, gating, and anesthetics in ion channels, Biophys. J. 94 (11) (2008) 4282–4298, https://doi.org/10.1529/BIOPHYSJ.107.120493, publisher: Cell Press.
[18] M. Tortora, S. Meloni, B.H. Tan, A. Giacomello, C.D. Ohl, C.M. Casciola, The interplay among gas, liquid and solid interactions determines the stability of surface nanobubbles, Nanoscale 12 (44) (2020) 22698–22709, https://doi.org/10.1039/D0NR05859A, publisher: Royal Society of Chemistry.
[19] A. Giacomello, R. Roth, Bubble formation in nanopores: a matter of hydrophobicity, geometry, and size, Adv. Phys. X 5 (1) (2020) 1817780, https://doi.org/10.1080/23746149.2020.1817780, publisher: Taylor & Francis.
[20] F. Gußmann, R. Roth, Bubble Gating in Biological Ion Channels: A Density Functional Theory Study, Phys. Rev. E 95 (6) (2017) 062407, https://doi.org/10.1103/PHYSREVE.95.062407/FIGURES/6/MEDIUM, publisher: American Physical Society.
[21] L. Guillemot, T. Biben, A. Galarneau, G. Vigier, É. Charlaix, Activated drying in hydrophobic nanopores and the line tension of water, Proc. Natl. Acad. Sci. USA 109 (48) (2012) 19557–19562, https://doi.org/10.1073/PNAS.1207658109/-/DCSUPPLEMENTAL, publisher: National Academy of Sciences.
[22] E. Lisi, M. Amabili, S. Meloni, A. Giacomello, C.M. Casciola, Self-recovery superhydrophobic surfaces: modular design, ACS Nano 12 (1) (2018) 359–367, https://doi.org/10.1021/ACSNANO.7B06438, publisher: American Chemical Society.
[23] A. Giacomello, M. Chinappi, S. Meloni, C.M. Casciola, Metastable wetting on superhydrophobic surfaces: continuum and atomistic views of the cassie-baxter-wenzel transition, Phys. Rev. Lett. 109 (22) (2012) 226102, https://doi.org/10.1103/PHYSREVLETT.109.226102/FIGURES/4/MEDIUM, publisher: American Physical Society.
[24] S. Prakash, E. Xi, A.J. Patel, Spontaneous recovery of superhydrophobicity on nanotextured surfaces, Proc. Natl. Acad. Sci. USA 113 (20) (2016) 5508–5513, https://doi.org/10.1073/PNAS.1521753113, arXiv:1511.07454, Publisher: National Academy of Sciences.
[25] A. Giacomello, S. Meloni, M. Chinappi, C.M. Casciola, Cassie-baxter and wenzel states on a nanostructured surface: phase diagram, metastabilities, and transition mechanism by atomistic free energy calculations, Langmuir 28 (29) (2012) 10764–10772, https://doi.org/10.1021/LA3018453, publisher: American Chemical Society.
[26] M. Amabili, Y. Grosu, A. Giacomello, S. Meloni, A. Zaki, F. Bonilla, A. Faik, C.M. Casciola, Pore morphology determines spontaneous liquid extrusion from nanopores, ACS Nano 13 (2) (2019) 1728–1738, https://doi.org/10.1021/acsnano.8b07818, publisher: American Chemical Society.
[27] Y.G. Bushuev, Y. Grosu, M.A. Chorażewski, S. Meloni, Subnanometer topological tuning of the liquid intrusion/extrusion characteristics of hydrophobic micropores, Nano Lett. 22 (6) (2022) 2164–2169, https://doi.org/10.1021/ACS.NANOLETT.1C02140, publisher: American Chemical Society.
[28] G. Paulo, A. Gubbiotti, Y. Grosu, S. Meloni, A. Giacomello, The impact of secondary channels on the wetting properties of interconnected hydrophobic nanopores, Commun. Phys. 6 (1) (2023) 1–6, https://doi.org/10.1038/s42005-023-01140-0, publisher: Nature Publishing Group.
[29] P. Zajdel, D.G. Madden, R. Babu, M. Tortora, D. Mirani, N.N. Tsyrin, L. Bartolomé, E. Amayuelas, D. Fairen-Jimenez, A.R. Lowe, M. Chorażewski, J.B. Leao, C.M. Brown, M. Bleuel, V. Stoudenets, C.M. Casciola, M. Echeverría, F. Bonilla, G. Grancini, S. Meloni, Y. Grosu, Turning Molecular Springs into Nano-Shock Absorbers: The Effect of Macroscopic Morphology and Crystal Size on the Dynamic Hysteresis of Water Intrusion–Extrusion into-from Hydrophobic Nanopores, ACS Appl. Mater. Interfaces 14 (23) (2022), https://doi.org/10.1021/ACSAMI.2C04314 26699–26713, Publisher: American Chemical Society.
[30] I. Khay, Chaplais Gérald, H. Nouali, C. Marichal, J. Patarin, Water intrusion-extrusion experiments in ZIF-8: impacts of the shape and particle size on the energetic performances, RSC Adv. 5 (40) (2015) 31514–31518.
[31] A. Demessence, C. Boissière, D. Grosso, P. Horcajada, C. Serre, G. Férey, G.J. Soler-Illia, C. Sanchez, Adsorption properties in high optical quality nanoZIF-8 thin films with tunable thickness, J. Mater. Chem. 20 (36) (2010) 7676–7681, https://doi.org/10.1039/C0JM00500B, publisher: the Royal Society of Chemistry.
[32] A. Le Bail, H. Duroy, J.L. Fourquet, Ab-initio structure determination of LiSbWO6 by X-ray powder diffraction, Mater. Res. Bull. 23 (3) (1988) 447–452, https://doi.org/10.1016/0025-5408(88)90019-0, publisher: Pergamon.
[33] J. Rodríguez-Carvajal, Recent advances in magnetic structure determination by neutron powder diffraction, Physica B, Condens. Matter 192 (1–2) (1993) 55–69, https://doi.org/10.1016/0921-4526(93)90108-I, publisher: North-Holland.
[34] M. Järvinen, Application of symmetrized harmonics expansion to correction of the preferred orientation effect, J. Appl. Crystallogr. 26 (4) (1993) 525–531, https://doi.org/10.1107/S0021889893001219, publisher: International Union of Crystallography.
[35] P.W. Stephens, Phenomenological model of anisotropic peak broadening in powder diffraction, J. Appl. Crystallogr. 32 (1999) 281–289.
[36] A.P. Thompson, H.M. Aktulga, R. Berger, D.S. Bolintineanu, W.M. Brown, P.S. Crozier, P.J. in 't Veld, A. Kohlmeyer, S.G. Moore, T.D. Nguyen, R. Shan, M.J. Stevens, J. Tranchida, C. Trott, S.J. Plimpton, LAMMPS - a flexible simulation tool for particle-based materials modeling at the atomic, meso, and continuum scales, Comput. Phys. Commun. 271 (2022) 108171, https://doi.org/10.1016/J.CPC.2021.108171, publisher: North-Holland.
[37] B. Zheng, M. Sant, P. Demontis, G.B. Suffritti, Force field for molecular dynamics computations in flexible ZIF-8 framework, J. Phys. Chem. C 116 (1) (2012) 933–938, https://doi.org/10.1021/JP209463A, publisher: American Chemical Society.
[38] J. Alejandre, G.A. Chapela, The surface tension of TIP4P/2005 water model using the Ewald sums for the dispersion interactions, J. Chem. Phys. 132 (1) (2010) 014701, https://doi.org/10.1063/1.3279128, publisher: American Institute of PhysicsAIP.
[39] L. Joly, C. Ybert, E. Trizac, L. Bocquet, Hydrodynamics within the electric double layer on slipping surfaces, Phys. Rev. Lett. 93 (25) (2004) 257805, https://doi.org/10.1103/PHYSREVLETT.93.257805/FIGURES/3/MEDIUM, arXiv: cond-mat/0411257, Publisher: American Physical Society.
[40] M. Tortora, P. Zajdel, A.R. Lowe, M. Chorażewski, J.B. Leão, G.V. Jensen, M. Bleuel, A. Giacomello, C.M. Casciola, S. Meloni, Y. Grosu, Giant negative compressibility by liquid intrusion into superhydrophobic flexible nanoporous frameworks, Nano Lett. 21 (7) (2021) 2848–2853, https://doi.org/10.1021/acs.nanolett.0c04941, publisher: American Chemical Society.
[41] C. Caddeo, D. Marongiu, S. Meloni, A. Filippetti, F. Quochi, M. Saba, A. Mattoni, Hydrophilicity and water contact angle on methylammonium lead iodide, Adv. Mater. Interfaces 6 (3) (2019) 1801173, https://doi.org/10.1002/ADMI.201801173, publisher: John Wiley & Sons, Ltd.
[42] T. Tian, M.T. Wharmby, J.B. Parra, C.O. Ania, D. Fairen-Jimenez, Role of crystal size on swing-effect and adsorption induced structure transition of ZIF-8, Dalton Trans. 45 (16) (2016) 6893–6900, https://doi.org/10.1039/c6dt00565a, publisher: Royal Society of Chemistry.
[43] S. Tanaka, K. Fujita, Y. Miyake, M. Miyamoto, Y. Hasegawa, T. Makino, S. Van Der Perre, J. Cousin Saint Remi, T. Van Assche, G.V. Baron, J.F. Denayer, Adsorption and diffusion phenomena in crystal size engineered ZIF-8 MOF, J. Phys. Chem. C 119 (51) (2015) 28430–28439, https://doi.org/10.1021/acs.jpcc.5b09520, publisher: American Chemical Society.
[44] J. Wolanin, L. Michel, D. Tabacchioni, J.M. Zanotti, J. Peters, I. Imaz, B. Coasne, M. Plazanet, C. Picard, Heterogeneous microscopic dynamics of intruded water in a superhydrophobic nanoconfinement: neutron scattering and molecular modeling, J. Phys. Chem. B 125 (36) (2021) 10392–10399, https://doi.org/10.1021/ACS.JPCB.1C06791, publisher: American Chemical Society.
[45] P. Zajdel, M. Chorażewski, J.B. Leão, G.V. Jensen, M. Bleuel, H.F. Zhang, T. Feng, D. Luo, M. Li, A.R. Lowe, M. Geppert-Rybczynska, D. Li, Y. Grosu, Inflation negative compressibility during intrusion-extrusion of a non-wetting liquid into a flexible nanoporous framework, J. Phys. Chem. Lett. 12 (20) (2021) 4951–4957, https://doi.org/10.1021/acs.jpclett.1c01305, publisher: American Chemical Society.
[46] Y. Zhu, J. Ciston, B. Zheng, X. Miao, C. Czarnik, Y. Pan, R. Sougrat, Z. Lai, C.E. Hsiung, K. Yao, I. Pinnau, M. Pan, Y. Han, Unravelling surface and interfacial structures of a metal-organic framework by transmission electron microscopy, Nat. Mater. 16 (5) (2017) 532–536, https://doi.org/10.1038/NMAT4852, publisher: Nature Publishing Group.
[47] Y.G. Bushuev, Y. Grosu, M.A. Chorażewski, S. Meloni, Effect of the topology on wetting and drying of hydrophobic porous materials, ACS Appl. Mater. Interfaces 14 (2022) 30067–30079, https://doi.org/10.1021/acsami.2c06039, publisher: American Chemical Society (ACS).

[48] A. Giacomello, C.M. Casciola, Y. Grosu, S. Meloni, Liquid intrusion in and extrusion from non-wettable nanopores for technological applications, Eur. Phys. J. B 94 (8) (Aug. 2021), https://doi.org/10.1140/epjb/s10051-021-00170-3, publisher: Springer Science and Business Media Deutschland GmbH.

[49] Y. Grosu, M. Li, Y.L. Peng, D. Luo, D. Li, A. Faik, J.M. Nedelec, J.P. Grolier, A highly stable nonhysteretic {Cu2(tebpz) MOF+water} molecular spring, ChemPhysChem 17 (21) (2016) 3359–3364, https://doi.org/10.1002/cphc.201600567, publisher: Wiley-VCH Verlag.

[50] L. Ronchi, A. Ryzhikov, H. Nouali, T.J. Daou, J. Patarin, Energetic performances of pure-silica DDR zeolite by high-pressure intrusion-extrusion of electrolyte aqueous solutions: a shock-absorber with huge absorbed energy, J. Phys. Chem. C 122 (5) (2018) 2726–2733, https://doi.org/10.1021/ACS.JPCC.7B10995, publisher: American Chemical Society.

[51] A. Ryzhikov, L. Ronchi, H. Nouali, T.J. Daou, J.L. Paillaud, J. Patarin, High-pressure intrusion-extrusion of water and electrolyte solutions in pure-silica LTA zeolite, J. Phys. Chem. C 119 (51) (2015) 28319–28325, https://doi.org/10.1021/ACS.JPCC.5B09861, publisher: American Chemical Society.

[52] L. Ronchi, A. Ryzhikov, H. Nouali, T.J. Daou, S. Albrecht, J. Patarin, Extra large pore opening CFI and DON-type zeosils for mechanical energy storage, Microporous Mesoporous Mater. 255 (2018) 211–219, https://doi.org/10.1016/J.MICROMESO.2017.07.039, publisher: Elsevier.

[53] L. Ronchi, Synthesis of hydrophobic zeolites for energetic applications, Ph.D. thesis, Université Haute-Alsace, 2017.

[54] L. Ronchi, A. Ryzhikov, H. Nouali, T.J. Daou, J. Patarin, Energetic performances of FER-type zeolite in the presence of electrolyte solutions under high pressure, Energy 130 (2017) 29–37, https://doi.org/10.1016/J.ENERGY.2017.04.128, publisher: Pergamon.

[55] L. Ronchi, H. Nouali, T.J. Daou, J. Patarin, A. Ryzhikov, Heterogeneous lyophobic systems based on pure silica ITH-type zeolites: high pressure intrusion of water and electrolyte solutions, New J. Chem. 41 (24) (2017) 15087–15093, https://doi.org/10.1039/C7NJ03470A, publisher: The Royal Society of Chemistry.

[56] L. Ronchi, A. Ryzhikov, H. Nouali, T.J. Daou, S. Albrecht, J. Patarin, Investigation of the energetic performance of pure silica BEC-type zeolite under high pressure water and 20 M LiCl intrusion-extrusion experiments, Microporous Mesoporous Mater. 254 (2017) 153–159, https://doi.org/10.1016/J.MICROMESO.2017.02.064, publisher: Elsevier.

[57] I. Khay, T.J. Daou, H. Nouali, A. Ryzhikov, S. Rigolet, J. Patarin, High pressure intrusion-extrusion of LiCl aqueous solutions in silicalite-1 zeolite: influence on energetic performances, J. Phys. Chem. C 118 (8) (2014) 3935–3941, https://doi.org/10.1021/JP4105163, publisher: American Chemical Society.

[58] C.W. Tsai, E.H. Langner, The effect of synthesis temperature on the particle size of nano-ZIF-8, Microporous Mesoporous Mater. 221 (2016) 8–13, https://doi.org/10.1016/j.micromeso.2015.08.041, publisher: Elsevier.

[59] D.N. Ta, H.K. Nguyen, B.X. Trinh, Q.T. Le, H.N. Ta, H.T. Nguyen, Preparation of nano-ZIF-8 in methanol with high yield, Can. J. Chem. Eng. 96 (7) (2018) 1518–1531, https://doi.org/10.1002/cjce.23155, publisher: Wiley-Liss Inc.